Conference on Modelling Fluid Flow (CMFF'25)
The 19th International Conference on Fluid Flow Technologies
Budapest, Hungary, August 26-August 29, 2025

Effects of Wall Slip on Large-Scale Flow in Turbulent Rayleigh–Bénard Convection

Sai Ravi Gupta Polasanapalli[1,2,3], Marten Klein[2,3], Heiko Schmidt[2,3]

[1] Corresponding Author. E-mail: polasana@btu.de
[2] Chair of Numerical Fluid and Gas Dynamics, Faculty of Mechanical Engineering, Electrical and Energy Systems, Brandenburg University of Technology Cottbus-Senftenberg. Siemens-Halske-Ring 15A, 03046 Cottbus, Germany
[3] Scientific Computing Lab, Energy Innovation Center, Brandenburg University of Technology Cottbus-Senftenberg. Universitätsstraße 22, 03046 Cottbus, Germany

ABSTRACT

The current study investigates the effects of surface boundary conditions—no-slip, free-slip, and finite-slip—on flow dynamics and heat transfer in turbulent Rayleigh–Bénard (RB) convection for different Prandtl numbers. Using a three-dimensional lattice Boltzmann method (LBM) solver in direct numerical simulation (DNS) mode, simulations are performed for three Prandtl numbers $Pr = 0.786, 4.38, 10$ and two Rayleigh numbers $Ra = 2 \times 10^6, 10^7$. The aim is to understand how surface conditions influence flow patterns, thermal mixing, and heat transfer efficiency in a cubic cavity with heated bottom and cooled top walls. Results show that free-slip conditions significantly enhance heat transfer, yielding higher Nusselt numbers due to thinner thermal boundary layers and stronger convective currents. In contrast, finite-slip conditions produce results similar to no-slip cases, indicating minimal impact for the slip lengths considered. The results demonstrate that surface boundary conditions play a role in modulating flow dynamics and heat transfer in RB convection.

Keywords: Lattice Boltzmann method (LBM), Navier-slip, Prandtl number effects, Rayleigh–Bénard (RB) convection, Surface boundary conditions, Turbulent flows.

NOMENCLATURE

H	$[m]$	Cavity height
Nu	$[-]$	Nusselt number
Pr	$[-]$	Prandtl number
Ra	$[-]$	Rayleigh number
TKE	$[m^2/s^2]$	Turbulent kinetic energy
g	$[m/s^2]$	acceleration due to gravity
rms	$[-]$	Root mean square
x, y, z	$[-]$	Coordinates
T_h	$[K]$	Bottom wall temperature
$T_\mathbf{c}$	$[K]$	Top wall temperature
$U_\mathbf{b}$	$[m/s]$	Free-fall velocity
ΔT	$[K]$	Temperature difference
β	$[1/K]$	Thermal expansion coefficient
κ	$[m^2/s]$	Thermal diffusivity
ν	$[m^2/s]$	Kinematic viscosity

1. INTRODUCTION

Surface coatings play a pivotal role in engineering applications, offering benefits such as drag reduction, corrosion resistance, wear resistance, and enhanced surface properties like thermal and electrical insulation. These coatings not only improve durability and efficiency but also passively influence scalar transfer in technical flows by modifying surface energy properties and altering boundary conditions. Flows over slippery surfaces are prevalent in both natural phenomena and industrial applications [1, 2]. Hydrophobic and super-hydrophobic surfaces, in particular, are widely used for drag reduction and self-cleaning in transportation systems. Numerically, the hydrophobicity of such surfaces can be modeled using tailored slip velocity boundary conditions.

A common mathematical framework for these applications involves the use of a finite slip length formulation. The Navier slip length, defined as the distance from the surface to the point where the extrapolated wall-parallel velocity component vanishes, is a standard choice [3]. A slip length of zero corresponds to a no-slip surface, while an infinite slip length represents a free-slip surface. Typical slip lengths range from 100 nm for hydrophobic surfaces to 100 μm for super-hydrophobic surfaces [4].

Copyright© Department of Fluid Mechanics, Budapest University of Technology and Economics and the Authors

Previous studies ([5, 6]) have explored the effects of slip length in turbulent channel flows, focusing on isotropic and anisotropic slip conditions for drag reduction. In the context of Rayleigh–Bénard (RB) convection, Mayeed et al. (2016) [7] demonstrated heat transfer enhancement using hydrophobic bottom and hydrophilic top walls, though their work was limited to two-dimensional flows and low Rayleigh numbers. Experimental studies by Wu et al. (2013) [8] further investigated the impact of surface wettability on RB convection.

In this study, we investigate the influence of various surface conditions on turbulent Rayleigh–Bénard convection, a canonical problem involving fluid confined in a cubic cavity with a heated bottom wall, a cooled top wall, and adiabatic side walls [9, 10]. Three-dimensional numerical simulations are performed using a lattice Boltzmann method (LBM) solver [11], which is well-suited for efficient upscaling to high Rayleigh number regimes with strong thermal forcing. The LBM solver operates in direct numerical simulation (DNS) mode, ensuring full-scale resolution of the flow dynamics. The primary objective is to examine the effects of no-slip, free-slip, and finite-slip boundary conditions on flow and heat transfer characteristics for fluids and chemical solvents with different Prandtl numbers.

2. FLOW SETUP AND CONFIGURATION

Figure 1 illustrates the schematic setup for Rayleigh–Bénard convection in a cubic cavity of dimensions $H \times H \times H$ in the x-, y-, and z-directions, respectively, where H is the height and serves as the characteristic length scale. The simulations are parameterized by the Rayleigh number, $Ra = \frac{\beta g H^3 \Delta T}{\nu \kappa}$, and the Prandtl number, $Pr = \frac{\nu}{\kappa}$. Here, β is the volumetric expansion coefficient of the fluid, g is the gravitational acceleration, and $\Delta T = T_h - T_c$ is the temperature difference across the cavity height H. ν and κ represent the kinematic viscosity and thermal diffusivity of the fluid, respectively.

The cubic cavity is bounded by walls on all sides. The bottom wall is heated and maintained at a higher temperature T_h, while the top wall is cooled and kept at a lower temperature T_c. The vertical side walls are treated as adiabatic, meaning no heat flux is allowed across them. For velocity boundary conditions, three configurations are considered: no-slip, free-slip, and Navier-slip. In the no-slip condition, all velocity components on the walls are set to zero. For the free-slip condition, the wall-normal velocity component is zero, while the wall-parallel components are specified using a Neumann boundary condition. In the finite-slip (Navier-slip) cases, the wall-normal velocity component is zero, and the wall-parallel components follow the Navier-slip condition: $u_s = l_s \frac{\partial u}{\partial n}$ as illustrated in Figure 2, where u is the wall-parallel velocity component, n is the wall-normal direction, and l_s is the slip length. The simulations are performed for the two Rayleigh numbers $Ra = 2 \times 10^6$, 10^7 and three Prandtl numbers $Pr = 0.786$ (air), 4.38 (water),10 (ethyl alcohol). For the finite-slip cases, isotropic slip lengths of $l_s = 0.00005, 0.0001, 0.0005$ are considered.

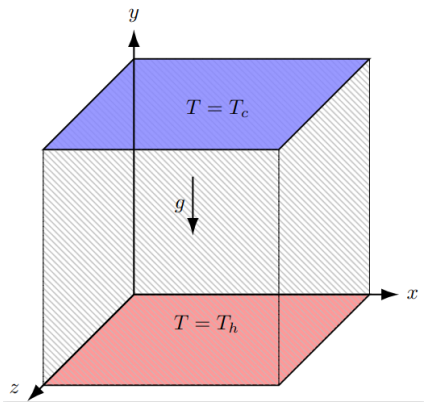

Figure 1. Schematic diagram of the cuboidal Rayleigh–Bénard convection set-up.

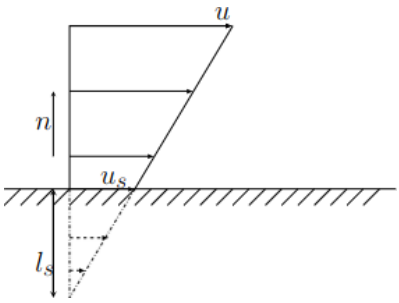

Figure 2. Schematic of the Navier-slip boundary condition parameterization based on a slip velocity u_s and a slip length l_s.

3. OVERVIEW OF THE NUMERICAL METHODOLOGY

The current study employs an off-lattice Boltzmann method (OLBM). The numerical solver implements the discrete velocity and temperature Boltzmann equations within the lattice Boltzmann method (LBM) framework to simulate flow and thermal fields. The implementation is based on a finite-difference approach, specifically designed for non-isothermal flows under the linear Oberbeck–Boussinesq approximation. To enhance numerical stability, the LBM collision term is treated implicitly. Time integration of the LBM equations is performed using a characteristic-based Lax–Wendroff scheme, while the advection terms are discretized using an explicit second-order central-difference scheme. To mitigate oscillations arising from non-dispersive central difference schemes, a sixth-order compact spatial filter is applied. The solver has been validated through various benchmark problems in earlier studies [11, 12, 13], and the same solver is utilized for the present simulations.

Copyright© Department of Fluid Mechanics, Budapest University of Technology and Economics and the Authors

Here, a stretched grid to achieve finer resolution near the wall boundaries, ensuring accurate capture of boundary layer dynamics. Initial perturbations, analogous to those proposed by Schoppa and Hussain (2000) [14], are introduced to the conductive initial condition. These finite-amplitude perturbations are designed to trigger convective instabilities, accelerating the transition from the initial state.

4. RESULTS

In a previous study, preliminary results on the influence of different surface boundary conditions (no-slip, free-slip, and finite Navier-slip) and varying slip lengths on RB convection had been obtained for a fixed Rayleigh number $Ra = 2 \times 10^6$ and Prandtl number $Pr = 4.38$. In the present study, we extend this analysis to explore the effects of surface boundary conditions on RB convection for fluids with different Prandtl numbers ($Pr = 0.786, 4.38, 10$). Statistical data were collected over sufficiently long time periods to ensure statistical independence. The analysis includes spanwise and time-averaged isotherm and flow pattern contours, as well as profiles of mean temperature $\langle T \rangle$, turbulent kinetic energy (TKE), and root mean square (RMS) fluctuation of temperature (T_{rms}) along the cavity height for each case. The impact on heat transfer is quantified using the Nusselt number (Nu). Temperature is normalized by $\Delta T = T_h - T_c$. Velocity components are normalized using the free-fall velocity $U_b = \sqrt{\beta g \Delta T H}$ as the bulk velocity scale. TKE and T_{rms} are normalized using U_b^2 and ΔT, respectively.

4.1. Effect on flow and thermal patterns

The formation of convection rolls or vortex modes is discussed in this section for different surface boundary conditions for $Ra = 2 \times 10^6$ and varying Pr. Additionally, results are presented for $Ra = 10^7$ and $Pr = 4.38$. Instantaneous flow contours reveal multiple chaotic flow patterns for no-slip and finite-slip boundary conditions, whereas a single large vortex is observed for free-slip cases. Flow reversal behavior is evident in instantaneous contours for all configurations except the free-slip (FS) case. Figures 3 - 11 present spanwise and time-averaged isotherm and streamline contours, illustrating the temperature distribution and flow patterns across the domain. While the x- and z-directions are geometrically equivalent in our cubic domain, the choice of spanwise averaging along the z-direction is made for consistency in visualization. Arrows indicate flow direction, with their lengths representing velocity magnitude, while the background color reflects the temperature field. The vortex patterns arise due to the buoyancy force generated by the temperature gradient between the top and bottom walls. In RB convection, the structure of these rolls typically depends on the aspect ratio of the domain and significantly influences heat transfer rates. In this study, the aspect ratio is fixed at 1 for all simulations. The surface boundary conditions induce substantial changes in both the flow and thermal fields.

A finite slip length of $l_s = 0.0005$ is considered for slip conditions for all Prandtl number cases. The results corresponding to $Pr = 4.38$ are presented in Figures 3 - 5 for different surface conditions. For $Pr = 4.38$ and 10, the flow patterns under no-slip and finite-slip conditions exhibit a (2, 2) vortex mode, characterized by two vortices along each horizontal and vertical direction. Usually, the (M, N) vortex mode denotes a flow pattern with M vortices in the horizontal plane and N vortices along the vertical direction. The (2, 2) vortex mode is attributed to the relatively low thermal diffusivity compared to momentum diffusivity at higher Prandtl numbers. As a result, heat is transported more slowly than momentum, and the flow is dominated by viscous effects. The results corresponding to $Pr = 0.786$ are presented in Figures 6 - 8 for different surface conditions. In contrast to higher Prandtl number cases, for the lower Prandtl number ($Pr = 0.786$), the flow under no-slip and finite-slip conditions is dominated by a single large diagonal vortex, accompanied by two smaller vortices near the other corners. This behavior arises because thermal diffusion dominates at lower Prandtl numbers, allowing heat to diffuse more rapidly than momentum. The weaker momentum diffusion promotes the formation of larger coherent structures, while the smaller corner vortices result from local recirculation effects and nonlinear interactions near the boundaries. Notably, higher velocity magnitudes are observed for the lower Prandtl number case, with velocity magnitudes decreasing as the Prandtl number increases. For free-slip boundary conditions, a single large vortex is observed across all Prandtl numbers. This is consistent with the reduced frictional resistance at the boundaries, which allows the flow to organize into a more coherent, large-scale structure.

The results for $Ra = 10^7$ and $Pr = 4.38$ are illustrated in Figures 9 - 11, showcasing surface conditions. Two different finite-slip lengths ($l_s = 0.0001$ and 0.00005) are considered in the simulations. At the higher Rayleigh number $Ra = 10^7$, the flow becomes more turbulent, and the influence of buoyancy forces dominates over viscous effects. Under no-slip and finite-slip conditions, the flow patterns are characterized by a single large diagonal vortex accompanied by two smaller corner vortices, even for the higher Prandtl number $Pr = 4.38$. This behavior is attributed to the strong buoyancy forces and turbulent mixing at higher Ra, which overcome the stabilizing effect of viscosity. The two smaller corner vortices are secondary flows driven by the interaction of the primary vortex with the boundaries. While the no-slip and finite-slip cases exhibit similar flow patterns, the finite-slip case with $l_s = 0.00005$ results in lower velocity magnitudes compared to the no-slip case. Simulations for free-slip boundary conditions at $Ra = 10^7$ are forthcoming and will be addressed

Copyright© Department of Fluid Mechanics, Budapest University of Technology and Economics and the Authors

elsewhere.

4.2. Effect on flow and thermal statistics

In this section, the variation of first-order and second-order statistical quantities along the cavity height is presented for different boundary conditions. Horizontal (x-z plane) averages of statistical quantities are presented in Figures 12 - 15 , providing a detailed understanding of the spatial distribution of flow and thermal properties in the Rayleigh-Bénard convection. Figures 12, 13 show the non-dimensionalized mean temperature profiles along the cavity height for $Ra = 2 \times 10^6$ and various Prandtl numbers (Pr = 0.786, 4.38, and 10). The mean temperature profiles for free-slip cases exhibit steeper gradients near the walls compared to no-slip and finite-slip conditions. This is due to the higher flow velocities near the walls in the free-slip configurations, which result in thinner thermal boundary layers and enhanced heat transfer. The finite-slip profiles are similar to those of the no-slip case, indicating that the slip length considered here (l_s = 0.0005) has a small effect on the thermal boundary layer. The thermal diffusion is dominant in the lower Prandtl number (Pr = 0.786) cases, resulting in smoother temperature profiles.

The profiles of non-dimensionalized turbulent kinetic energy (TKE) along the cavity height are presented in Figure 14 for different Prandtl numbers (Pr = 0.786, 4.38, and 10) and boundary conditions. TKE is a key measure of the intensity of turbulent fluctuations in the flow. In free-slip cases, the fluid near the walls experiences minimal frictional resistance, allowing for higher flow velocities and stronger turbulent fluctuations. As a result, the TKE values are significantly larger for free-slip boundary conditions compared to no-slip and finite-slip cases across all Prandtl numbers. The absence of wall friction in free-slip configurations enhances the turbulence intensity, leading to more mixing within the flow. This behavior is consistent with the observed steeper temperature gradients and higher heat transfer rates in free-slip cases, as discussed earlier. The Prandtl number influences the TKE distribution along the vertical coordinate. At lower Prandtl numbers (Pr = 0.786), thermal diffusion dominates over momentum diffusion, resulting in larger flow velocities and stronger turbulent fluctuations. Consequently, the TKE values are higher for the Pr = 0.786 case compared to the higher Prandtl number cases. The difference between finite-slip and no-slip cases is also more pronounced at lower Prandtl numbers, with finite-slip conditions showing slightly larger TKE values due to the reduced frictional resistance at the walls. For higher Prandtl numbers, the TKE values are lower due to the increased viscous damping of turbulent fluctuations. The difference between no-slip and finite-slip cases is relatively small, indicating that the effect of partial slip on turbulence intensity diminishes for higher Prandtl numbers.

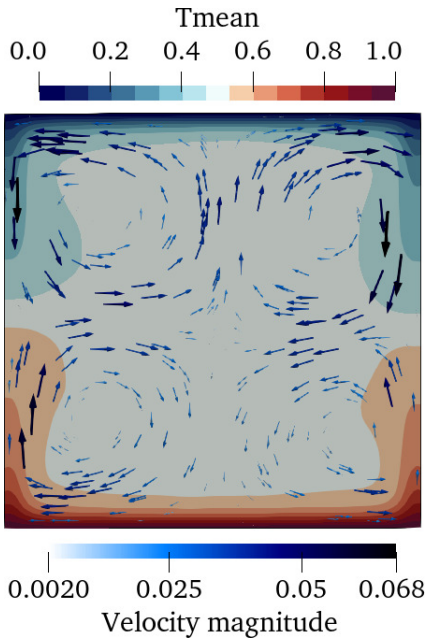

Figure 3. Time- and spanwise-averaged mean velocity vectors (arrows) and temperature distribution (colored contours) for the no-slip case at $Ra = 2 \times 10^6$ and Pr = 4.38.

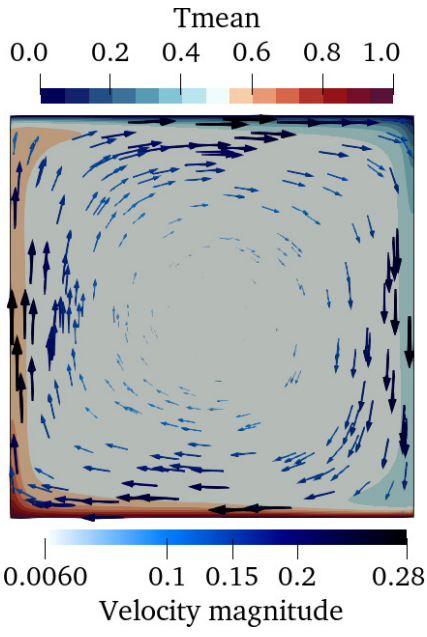

Figure 4. Time- and spanwise-averaged mean velocity vectors (arrows) and temperature distribution (colored contours) for the free-slip case at $Ra = 2 \times 10^6$ and Pr = 4.38.

Copyright© Department of Fluid Mechanics, Budapest University of Technology and Economics and the Authors

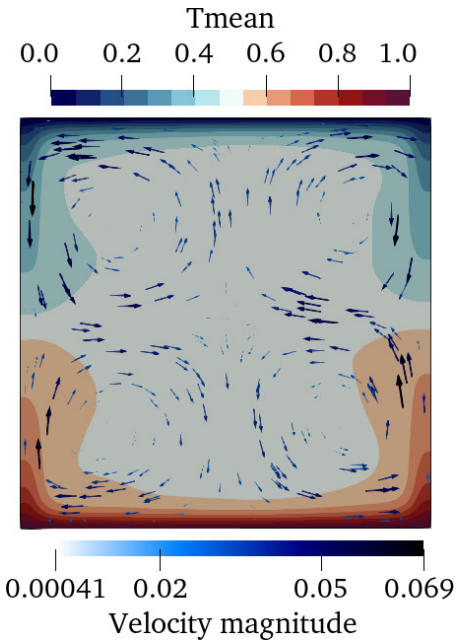

Figure 5. Time- and spanwise-averaged mean velocity vectors (arrows) and temperature distribution (colored contours) for the finite-slip case at $Ra = 2 \times 10^6$ and $Pr = 4.38$.

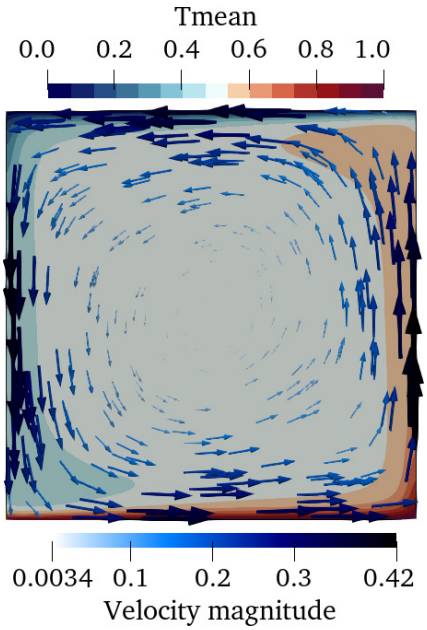

Figure 7. Time- and spanwise-averaged mean velocity vectors (arrows) and temperature distribution (colored contours) for the free-slip case at $Ra = 2 \times 10^6$ and $Pr = 0.786$.

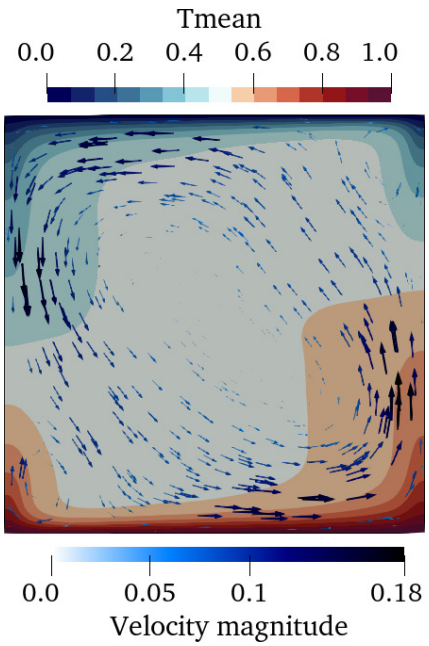

Figure 6. Time- and spanwise-averaged mean velocity vectors (arrows) and temperature distribution (colored contours) for the no-slip case at $Ra = 2 \times 10^6$ and $Pr = 0.786$

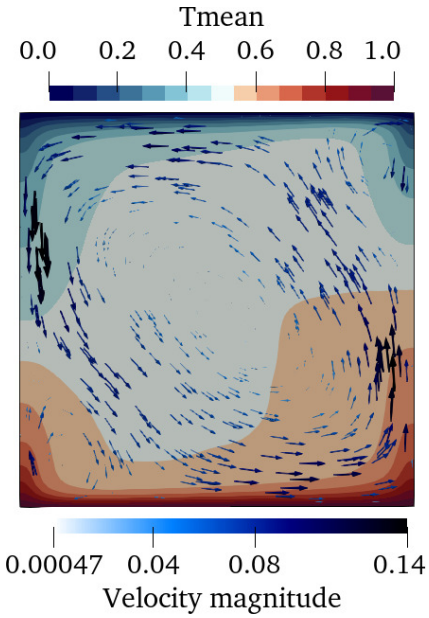

Figure 8. Time- and spanwise-averaged mean velocity vectors (arrows) and temperature distribution (colored contours) for the finite-slip case at $Ra = 2 \times 10^6$ and $Pr = 0.786$.

Copyright© Department of Fluid Mechanics, Budapest University of Technology and Economics and the Authors

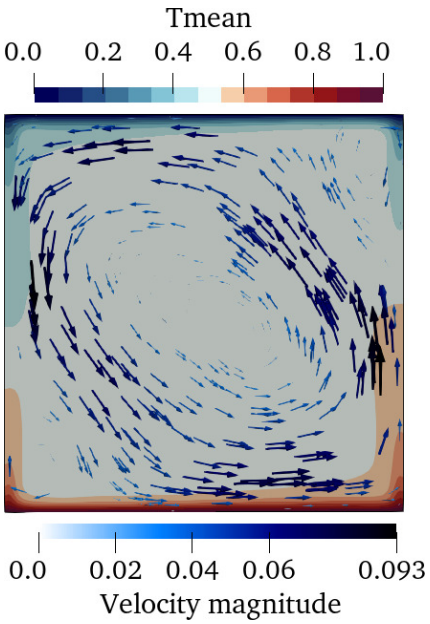

Figure 9. Time- and spanwise-averaged mean velocity vectors (arrows) and temperature distribution (colored contours) for the no-slip case at $Ra = 10^7$ and $Pr = 4.38$.

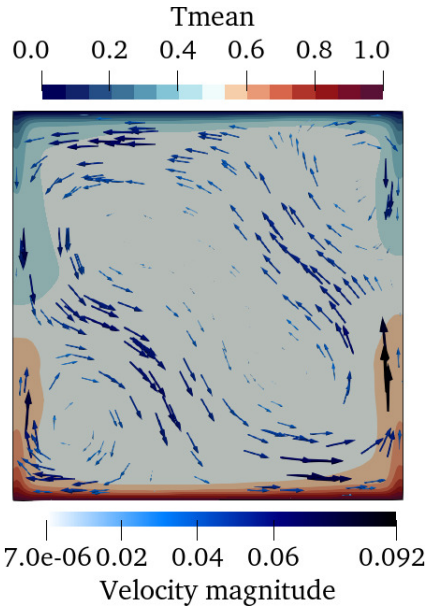

Figure 10. Time- and spanwise-averaged mean velocity vectors (arrows) and temperature distribution (colored contours) for the finite-slip with $l_s = 0.0001$ case at $Ra = 2 \times 10^6$ and $Pr = 4.38$.

The profiles of non-dimensionalized root mean square (RMS) temperature fluctuations (T_{rms}) along the cavity height are shown in Figure 15 for different Prandtl numbers and boundary conditions at $Ra = 2 \times 10^6$. The T_{rms} profiles provide insights into the intensity of thermal fluctuations and the efficiency of thermal mixing in Rayleigh-Bénard con-

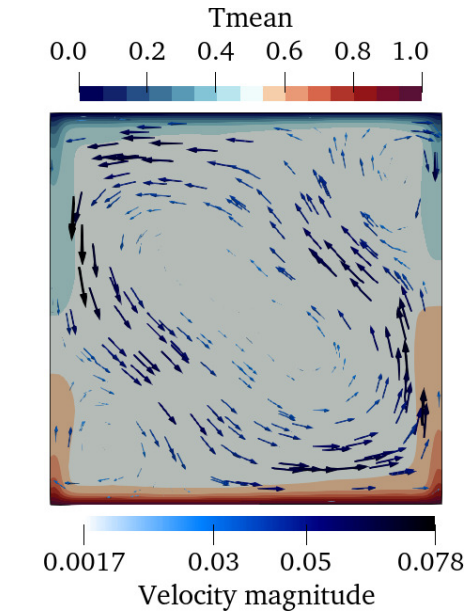

Figure 11. Time- and spanwise-averaged mean velocity vectors (arrows) and temperature distribution (colored contours) for the finite-slip with $l_s = 0.00005$ case at $Ra = 2 \times 10^6$ and $Pr = 4.38$.

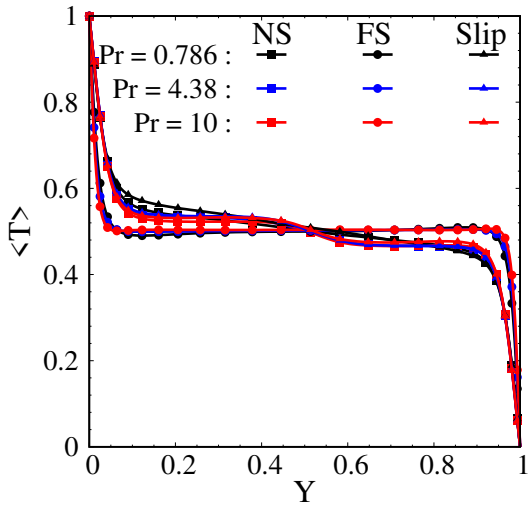

Figure 12. Vertical profiles of the mean temperature.

vection. The steeper gradients near the walls in free-slip cases indicate a thinner thermal boundary layer, which is consistent with the higher heat transfer rates observed in these configurations. The higher T_{rms} values near the walls in free-slip cases are because of intense thermal mixing. The difference between finite-slip and no-slip cases is small, indicating that the slip length considered here ($l_s = 0.00050$) has a minimal effect on the thermal fluctuations. The T_{rms} profiles look smoother for lower Prandtl numbers because of the stronger diffusion effects.

Copyright© Department of Fluid Mechanics, Budapest University of Technology and Economics and the Authors

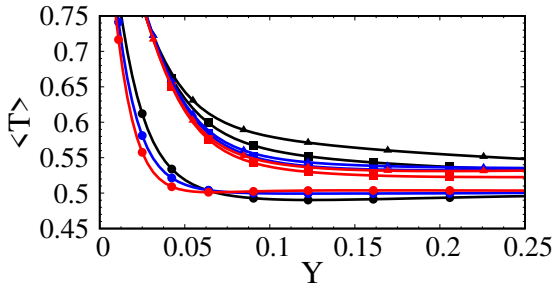

Figure 13. Zoomed-in view of the mean temperature profiles from Figure 12 showing the vicinity of the bottom wall.

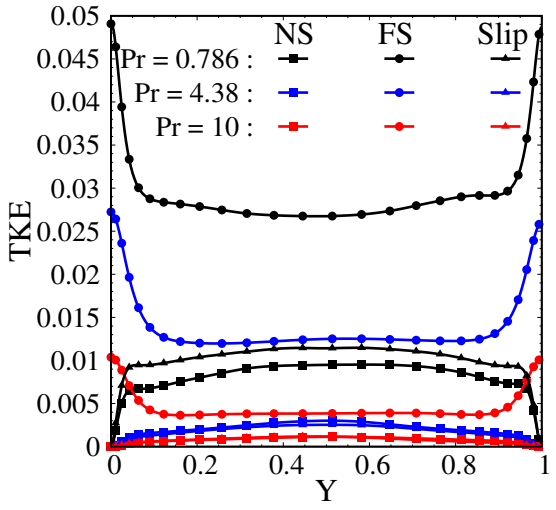

Figure 14. Vertical profiles of the TKE.

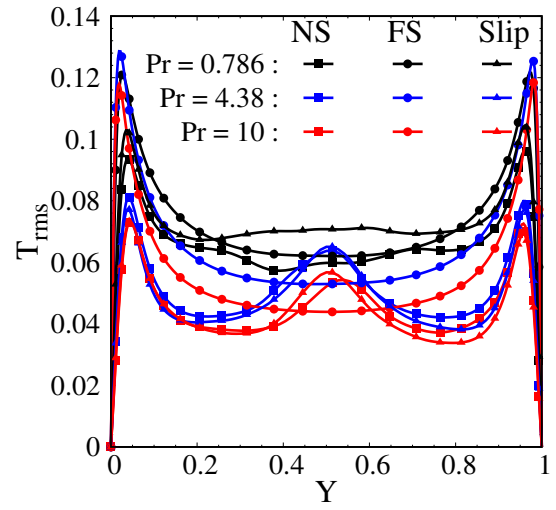

Figure 15. Vertical profiles of the RMS fluctuation temperature.

4.3. Effect on heat transfer

The Nusselt number (Nu) is a key dimensionless parameter used to quantify the heat transfer rate in convective systems. In this study, the overall mean Nusselt number is computed as the area average of $Nu = -\frac{\partial \langle T \rangle}{\partial y} / \left(\frac{\Delta T}{H}\right)$ over the top and bottom walls. The Nusselt number provides a measure of the efficiency of convective heat transfer relative to conductive heat transfer.

The Nusselt numbers for different cases are presented in Table 1. In free-slip cases, the fluid experiences no frictional resistance at the walls, allowing for higher flow velocities near those boundaries. This results in a thinner thermal boundary layer (see Figure 13), which significantly enhance the heat transfer rate. The free-slip condition enables the fluid to move more freely near the walls, increasing thermal gradients and promoting stronger convective heat transfer. As a result, the free-slip condition consistently yields higher Nusselt numbers compared to no-slip and finite-slip conditions across all Prandtl numbers investigated. Notably, the enhancement in heat transfer is most pronounced for $Pr = 10$, where the Nusselt number increases 170% compared to the no-slip case. This is attributed to the combined effects of reduced viscous damping and enhanced thermal gradients at higher Prandtl numbers. Finite-slip boundary conditions, which allow partial slip at the walls, result in heat transfer rates that are nearly identical to those observed for no-slip conditions. This suggests that the finite-slip length considered here ($l_s = 0.0005$) is insufficient to significantly alter the flow dynamics or heat transfer characteristics compared to the no-slip condition. At the higher Rayleigh number $Ra = 10^7$ and $Pr = 4.38$, the heat transfer rates are significantly higher due to the increased buoyancy-driven turbulence. These results indicate that the finite-slip boundary conditions result in only minor changes in heat transfer at high Rayleigh numbers. A small increment in the Nusselt number is observed for the finite-slip case $l_s = 0.0001$. Even at higher turbulent Rayleigh numbers, the effect of partial slip on heat transfer remains limited for the slip lengths considered in this study.

Table 1. Nusselt number obtained from the different boundary conditions simulations.

Ra	Pr	Walls	Nu
2×10^6		No-slip	10.27
2×10^6	0.786	Free-slip	21.43
2×10^6		Slip $l_s = 0.0005$	10.30
2×10^6		No-slip	9.97
2×10^6	4.38	Free-slip	19.99
2×10^6		Slip $l_s = 0.0005$	9.90
2×10^6		No-slip	9.81
2×10^6	10	Free-slip	26.55
2×10^6		Slip $l_s = 0.0005$	9.75
10^7		No-slip	16.76
10^7	4.38	Slip $l_s = 0.0001$	17.27
10^7		Slip $l_s = 0.00005$	16.74

Copyright© Department of Fluid Mechanics, Budapest University of Technology and Economics and the Authors

5. CONCLUSION

This study investigates the effects of different surface boundary conditions—no-slip, free-slip, and finite-slip—on flow dynamics and heat transfer in turbulent Rayleigh–Bénard convection for various Prandtl numbers (Pr = 0.786, 4.38, and 10). Three-dimensional numerical simulations were performed using an off-lattice Boltzmann method solver in DNS mode. Free-slip boundary conditions consistently produce a single large vortex across all Prandtl numbers, as the absence of wall friction allows for stronger convective currents and more efficient thermal mixing. Free-slip conditions significantly enhance heat transfer, producing higher Nusselt numbers due to thinner thermal boundary layers and stronger convective currents, while finite-slip conditions yield results similar to those of no-slip cases, indicating minimal impact for the slip lengths considered. Flow patterns vary with Prandtl number, with higher Pr fluids forming smaller vortices and lower Pr fluids exhibiting larger coherent structures. At $Ra = 10^7$, increased turbulence leads to a large vortex flow pattern, even for higher Pr. These findings highlight the critical role of surface conditions in modulating flow dynamics and heat transfer, with free-slip surfaces offering significant thermal performance improvements. Future studies will explore the effect of slip on larger aspect ratio domains and conduct detailed analyses of boundary layers and energy budgets to further advance practical applications.

ACKNOWLEDGEMENT

This research is supported by the German Federal Government, the Federal Ministry of Research, Technology and Space, and the State of Brandenburg within the framework of the joint project EIZ: Energy Innovation Center (project numbers 85056897 and 03SF0693A) with funds from the Structural Development Act for coal-mining regions. The authors gratefully acknowledge the provision of computing resources by the National High Performance Computing Alliance (NHR@ZIB and NHR-NORD@Göttingen) under the project number bbi00022.

REFERENCES

[1] Tritton, D., 1975, "Internally heated convection in the atmosphere of Venus and in the laboratory", *Nature*, Vol. 257 (5522), pp. 110–112.

[2] Choi, C.-H., and Kim, C.-J., 2006, "Large slip of aqueous liquid flow over a nanoengineered superhydrophobic surface", *Physical review letters*, Vol. 96 (6), p. 066001.

[3] Rothstein, J. P., 2010, "Slip on superhydrophobic surfaces", *Annual review of fluid mechanics*, Vol. 42 (1), pp. 89–109.

[4] Voronov, R. S., Papavassiliou, D. V., and Lee, L. L., 2008, "Review of fluid slip over superhydrophobic surfaces and its dependence on the contact angle", *Industrial & Engineering Chemistry Research*, Vol. 47 (8), pp. 2455–2477.

[5] Min, T., and Kim, J., 2004, "Effects of hydrophobic surface on skin-friction drag", *Physics of Fluids*, Vol. 16 (7), pp. L55–L58.

[6] Fukagata, K., Kasagi, N., and Koumoutsakos, P., 2006, "A theoretical prediction of friction drag reduction in turbulent flow by superhydrophobic surfaces", *Physics of fluids*, Vol. 18 (5).

[7] Mayeed, M. S., Patnaik, S. S., and Mitchell, R., 2016, "Heat Transfer Enhancement Using Miniaturized Channel Sections With Surface Modifications", *Proceedings of the ASME 2016 IMECE2016*, ASME, USA.

[8] Wu, C. H., Huang, Y. S., Kuo, L. S., and Chen, P. H., 2013, "The effects of boundary wettability on turbulent natural convection heat transfer in a rectangular enclosure", *International Journal of Heat and Mass Transfer*, Vol. 63, pp. 249–254.

[9] Scheel, J. D., Emran, M. S., and Schumacher, J., 2013, "Resolving the fine-scale structure in turbulent Rayleigh–Bénard convection", *New Journal of Physics*, Vol. 15 (11), p. 113063.

[10] Wagner, S., and Shishkina, O., 2015, "Heat flux enhancement by regular surface roughness in turbulent thermal convection", *Journal of Fluid Mechanics*, Vol. 763, pp. 109–135.

[11] Polasanapalli, S. R. G., and Anupindi, K., 2022, "Large-eddy simulation of turbulent natural convection in a cylindrical cavity using an off-lattice Boltzmann method", *Physics of Fluids*, Vol. 34 (3), p. 035125.

[12] Polasanapalli, S. R. G., and Anupindi, K., 2024, "Turbulent mixed convection in a horizontal cylindrical cavity with the off-lattice Boltzmann method", *International Journal of Heat and Mass Transfer*, Vol. 225, p. 125395.

[13] Polasanapalli, S. R. G., Klein, M., and Schmidt, H., 2024, "Towards stochastic subgrid-scale modeling of turbulent thermal convection in an under-resolved off-lattice Boltzmann method", *PAMM*, Vol. 24 (1), p. e202300223.

[14] Schoppa, W., and Hussain, F., 2000, "Coherent structure dynamics in near-wall turbulence", *Fluid Dynamics Research*, Vol. 26 (2), pp. 119–139.

Copyright© Department of Fluid Mechanics, Budapest University of Technology and Economics and the Authors